

ARTICLE

<https://doi.org/10.1038/s41467-019-12314-2>

OPEN

# Perfect proton selectivity in ion transport through two-dimensional crystals

L. Mogg<sup>1,2</sup>, S. Zhang<sup>2,3</sup>, G.-P. Hao<sup>2,4</sup>, K. Gopinadhan<sup>2,5</sup>, D. Barry<sup>2</sup>, B.L. Liu<sup>6</sup>, H.M. Cheng<sup>6</sup>, A.K. Geim<sup>1,2</sup> & M. Lozada-Hidalgo<sup>1,2</sup>

Defect-free monolayers of graphene and hexagonal boron nitride are surprisingly permeable to thermal protons, despite being completely impenetrable to all gases. It remains untested whether small ions can permeate through the two-dimensional crystals. Here we show that mechanically exfoliated graphene and hexagonal boron nitride exhibit perfect Nernst selectivity such that only protons can permeate through, with no detectable flow of counterions. In the experiments, we use suspended monolayers that have few, if any, atomic-scale defects, as shown by gas permeation tests, and place them to separate reservoirs filled with hydrochloric acid solutions. Protons account for all the electrical current and chloride ions are blocked. This result corroborates the previous conclusion that thermal protons can pierce defect-free two-dimensional crystals. Besides the importance for theoretical developments, our results are also of interest for research on various separation technologies based on two-dimensional materials.

<sup>1</sup>National Graphene Institute, The University of Manchester, Manchester M13 9PL, UK. <sup>2</sup>Department of Physics and Astronomy, The University of Manchester, Manchester M13 9PL, UK. <sup>3</sup>Key Laboratory for Green Chemical Technology of Ministry of Education, Collaborative Innovation Center of Chemical Science and Engineering, School of Chemical Engineering and Technology, Tianjin University, Tianjin 300072, China. <sup>4</sup>State Key Laboratory of Fine Chemicals, School of Chemical Engineering, Dalian University of Technology, Dalian 116024, China. <sup>5</sup>Department of Physics, Indian Institute of Technology Gandhinagar, Gandhinagar, Gujarat 382355, India. <sup>6</sup>Shenzhen Graphene Center Tsinghua-Berkeley Shenzhen Institute, Tsinghua University, 1001 Xueyuan Road, Shenzhen 518055, China. Correspondence and requests for materials should be addressed to S.Z. (email: [sheng.zhang@tju.edu.cn](mailto:sheng.zhang@tju.edu.cn)) or to A.K.G. (email: [geim@manchester.ac.uk](mailto:geim@manchester.ac.uk)) or to M.L.-H. (email: [marcelo.lozadahidalgo@manchester.ac.uk](mailto:marcelo.lozadahidalgo@manchester.ac.uk))

Proton transport through two-dimensional (2D) crystals has recently been studied, both experimentally and theoretically<sup>1–9</sup>. As for the experiment, it was found that proton permeation through mechanically exfoliated crystals is thermally activated with energy barriers of  $\approx 0.8$  eV for graphene and  $\approx 0.3$  eV for monolayer hexagonal boron nitride (hBN)<sup>1</sup>. Further measurements using deuterons, nuclei of the hydrogen isotope deuterium, show that quantum oscillations raise the energy of incoming protons by  $0.2$  eV<sup>2</sup>. This correction yielded the total barriers of  $\approx 0.5$  eV for monolayer hBN and  $\approx 1$  eV for graphene. From a theoretical perspective, the latter value is notably lower (by at least 30% but typically a factor of 2) than that found in density-functional calculations for graphene<sup>3–7</sup>. To account for the difference, a recent theory suggests that graphene can be partially hydrogenated during the measurements, which makes its lattice slightly sparser; thus, making it more permeable to protons<sup>8,9</sup>. An alternative explanation put forward attributes the observed proton currents to atomic-scale lattice defects, including vacancies<sup>10,11</sup>. This was argued on the basis of ion-selectivity measurements using chemical-vapor-deposited (CVD) graphene<sup>11</sup>. Indeed, CVD graphene is known to possess a large density of atomic-scale defects that appear during growth<sup>12–14</sup>. Such defects are generally absent in mechanically exfoliated 2D crystals, which was proven conclusively in gas-leak experiments using the so-called nanoballoons<sup>15–17</sup>. Even a single angstrom-sized vacancy per micrometer-size area could be detected in those experiments<sup>16,17</sup>. Whereas it is plausible that vacancies and similar defects played a dominant role in experiments using CVD graphene<sup>10,11</sup>, extrapolation of those results to mechanically exfoliated 2D crystals is unjustifiable. To resolve the controversy, it is crucial to carry out similar ion-selectivity studies using mechanically exfoliated crystals with little or no defects<sup>1,2,15</sup>.

Here we report ion-selectivity measurements using mechanically exfoliated graphene and hBN monolayers. The crystals are found to be perfectly selective with respect to protons. The latter can permeate through the 2D membranes, whereas even such small ions as chlorine are blocked. The results support the previous conclusion<sup>1</sup> that transport of thermal protons through high-quality graphene and hBN occurs through their bulk and does not involve vacancies and other atomic-scale defects.

## Results

**Device fabrication and characterization.** The investigated devices were fabricated using monolayer graphene and mono- and bilayer hBN crystals that were isolated by micromechanical cleavage<sup>18</sup> (see Methods and Supplementary Fig. 1). The crystals were suspended over microfabricated apertures ( $2\ \mu\text{m}$  in diameter) etched in free-standing silicon-nitride (SiN) membranes<sup>1</sup> (Supplementary Fig. 2). A prefabricated polymer washer with a  $10\ \mu\text{m}$ -diameter hole was then transferred on top of the crystal so that the hole was aligned with the aperture in the SiN membrane (Supplementary Fig. 2). The assembly was baked at  $\sim 150^\circ\text{C}$ , to ensure that the washer firmly clamped the 2D crystal to SiN and sealed the crystal edges, to prevent any possible leak along the substrate. In a series of control experiments, we checked that there were no microscopic defects in our exfoliated 2D crystals by employing the approach described in refs. <sup>15,16</sup> and previously also used in our experiments<sup>1</sup>. To this end, we made hBN and graphene membranes to cover micrometer-sized cavities etched in an oxidized Si wafer and tested the enclosures for possible gas leaks (see inset Fig. 1b and Supplementary Section ‘Leak tests using nanoballoons’). Even a single vacancy would be detectable in these measurements<sup>16,17</sup>, but neither of the dozens of tested 2D crystals showed such leakage (Supplementary Fig. 3). In contrast,

similar devices made from CVD graphene normally exhibited notable gas permeation.

**Ion conductivity measurements.** The chips containing the individual 2D membranes (Supplementary Fig. 2) were then used to separate two compartments filled with hydrochloric acid (HCl) at chosen concentrations<sup>19</sup>. Electrical conductance through the membranes was probed using Ag/AgCl electrodes placed inside the compartments. Figure 1a shows the current density  $I$  as a function of applied voltage  $V$  for representative devices made from graphene and hBN. The  $I$ - $V$  response was linear, which allowed us to determine the areal conductivity  $\sigma = I/V$ . We found monolayer hBN to be the most conductive of the studied crystals, followed by bilayer hBN and monolayer graphene. For example, using  $1\ \text{M}$  HCl we found  $\sigma \approx 1,000\ \text{mS cm}^{-2}$  for monolayer hBN,  $\approx 40\ \text{mS cm}^{-2}$  for bilayer hBN and  $\approx 12\ \text{mS cm}^{-2}$  for monolayer graphene. The relative conductivities agree well with those found in the previous studies using Nafion (rather than HCl) as the proton-conducting medium<sup>1</sup>. Thicker crystals (e.g., bilayer graphene) exhibited no discernible conductance, again in agreement with the previous report<sup>1</sup>.

As monolayer hBN exhibited the highest conductivity, we focus our discussion below on this particular 2D material, as it allowed the most accurate ion-selectivity measurements (results for graphene are presented in Supplementary Information). Figure 1b shows  $\sigma$  found for hBN at various HCl concentrations (the same concentration was used in both compartments). For concentrations above  $1\ \text{mM}$ ,  $\sigma$  increased linearly with HCl concentration. At lower concentrations, the measured current was below our detection limit. The latter was determined by electrical leakage along surfaces of the liquid cell and was of the order of  $1\ \text{pA}$  as found using control devices with no holes in the SiN membranes<sup>19</sup>. In another control experiment, we used devices with the same SiN aperture but without a 2D crystal. They exhibited conductance at least  $\sim 1000$  times larger than that for the devices with graphene or hBN crystals covering the aperture (Supplementary Fig. 4). This demonstrates that the reported values of  $\sigma$  were limited by the relatively low ion permeation through 2D crystals and the series resistance due to the electrolyte itself could be neglected.

**Proton selectivity.** The measured conductivity could be due to either  $\text{H}^+$  or  $\text{Cl}^-$ , or both ions permeating through 2D crystals. For the purpose described in the introduction, it is necessary to determine the fraction of  $I$  carried by each of these species. Such fractions are usually referred to as transport numbers<sup>20</sup> ( $t_{\text{H}}$  and  $t_{\text{Cl}}$  for protons and chloride, respectively) and, by definition, they satisfy  $t_{\text{H}} + t_{\text{Cl}} \equiv 1$  and the inequality:  $0 \leq$  both  $t_{\text{H}}$  and  $t_{\text{Cl}} \leq 1$ . To find their values for our 2D membranes, we used the same setup as in the measurements discussed in Fig. 1 but with different HCl concentrations in the two compartments (inset of Fig. 2b). The concentration gradient drives both  $\text{H}^+$  and  $\text{Cl}^-$  ions towards equilibrium, from the high concentration ( $C_{\text{h}}$ ) compartment to the low concentration ( $C_{\text{l}}$ ) one. Therefore, the sign of the total ionic current at zero  $V$  indicates whether the majority carriers are protons (positive  $I$ ) or chloride ions (negative). Figure 2a shows typical  $I$ - $V$  characteristics for monolayer hBN devices and concentration ratio  $\Delta C \equiv C_{\text{h}}/C_{\text{l}} = 10$ . Independently of the absolute values of HCl concentrations, the zero  $V$  current was always positive, proving that the protons dominate ion transport through our membranes. The same behavior was found for graphene devices (Supplementary Fig. 5).

The force pushing ions across the membrane, due to the concentration gradient, can be counteracted by applying voltage

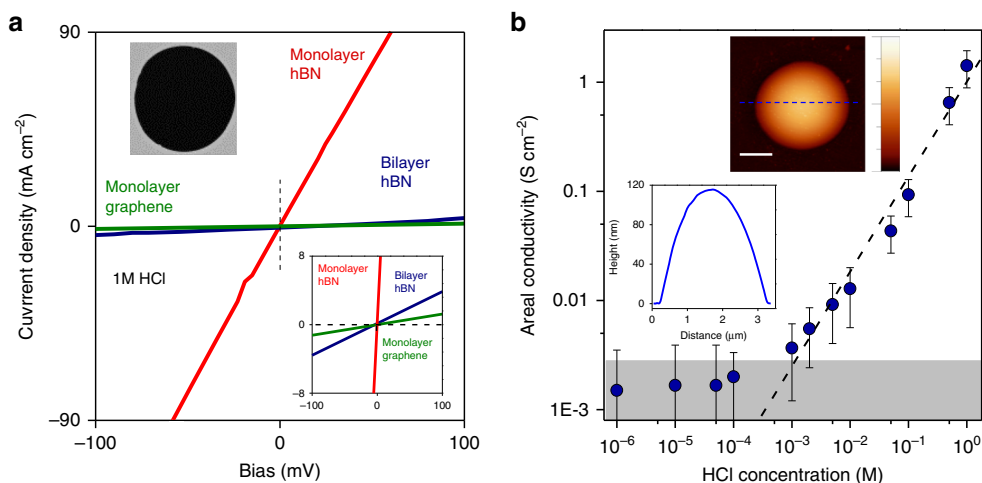


**Fig. 1** Proton transport through 2D crystals studied using aqueous solutions. **a** Examples of  $I$ - $V$  characteristics for 1 M HCl. Bottom inset: zoom-in. Top inset: electron micrograph of a suspended hBN membrane (aperture diameter, 2  $\mu\text{m}$ ). **b** Concentration dependence of the areal conductivity  $\sigma$  for monolayer hBN. Gray area indicates our detection limit given by parasitic leakage currents. Error bars: SD from different measurements. Dashed line: best linear fit to the data. Top inset: atomic force microscopy (AFM) height profile of an ‘inflated nanoballoon’. Here, graphene monolayer seals a micrometer-sized cavity containing pressurized Ar. The pressure difference across the membrane makes it to bulge up. Lateral scale bar, 1  $\mu\text{m}$ ; color scale, 130 nm. Bottom inset: AFM line trace taken along the blue dotted line in the top inset

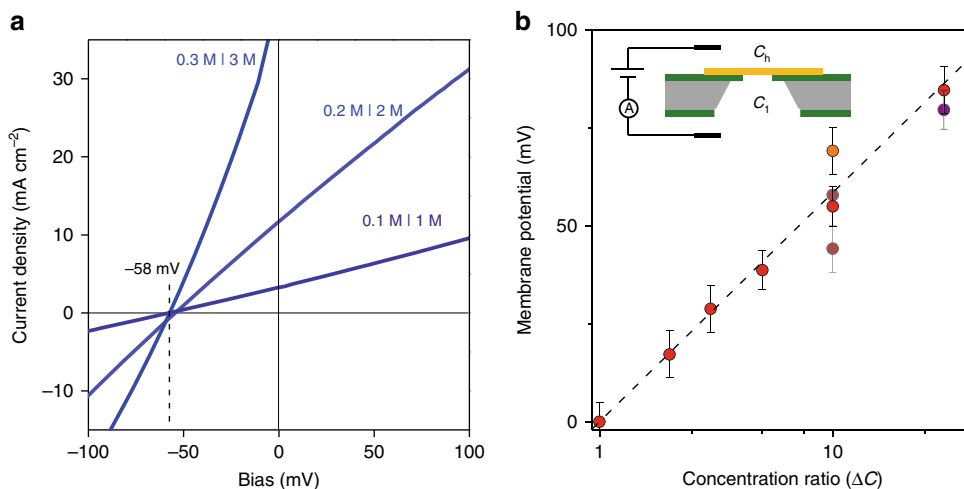


**Fig. 2** Proton selectivity. **a** Examples of  $I$ - $V$  characteristics for various HCl concentrations across a monolayer hBN membrane at a fixed  $\Delta C = 10$ . The current at zero voltage (intersection with the y axis) was always positive. The reversal potential  $V_0$  is given by the intersection of the  $I$ - $V$  curves with the x axis and was  $V_0 \approx -58 \text{ mV}$  as marked by the dotted line. **b**  $V_0$  for different  $\Delta C$  and four different hBN devices (symbols of different color). Error bars, SD from different measurements. The black line is given by Eq. (1) for  $t_H = 1$  and  $t_{Cl} = 0$ . Inset: Schematic of the experimental setup

$V$ . The value  $V_0$  at which the current becomes zero is known as the membrane or reversal potential and is given by the Nernst equation<sup>21</sup>

$$V_0 = (t_{Cl} - t_H)(k_B T/e) \ln(\Delta C) = -(2t_H - 1)(k_B T/e) \ln(\Delta C) \quad (1)$$

where  $k_B$  is the Boltzmann constant,  $T$  is the temperature and  $e$  is the elementary charge. If one of the transport numbers is unity, the other must be zero and, then, it is said that a membrane displays perfect Nernst selectivity. Figure 2a shows that for  $\Delta C = 10$ , the  $I$ - $V$  curves intersected the x-axis at the same  $V$ , which means that our membranes exhibited  $V_0 \approx -58 \text{ mV}$ , regardless of the absolute values of the HCl concentrations. This value is equal to  $-(k_B T/e) \ln(\Delta C = 10) \approx -58 \text{ meV}$  at our measurement temperature of  $\sim 20^\circ \text{C}$  and, therefore, the observation implies  $t_H \approx 1$

or, equivalently, that all the ionic current through the membrane is due to proton transport. Within our experimental accuracy, the same perfect selectivity was also found for graphene (Supplementary Fig. 5).

To corroborate the above result and obtain better statistics for the ion selectivity, we carried out similar measurements using different devices and several concentration ratios ranging from  $\Delta C = 1$  to 30 (Fig. 2b). For all of them, we found membrane potentials consistent with the perfect proton selectivity in Eq. (1). The best fit to the data in Fig. 2b yields  $t_H = 0.99 \pm 0.02$ , or  $t_H \approx 1$ . In control experiments, we verified our experimental approach using porous glass membranes. They allow large concentration gradients but provide no ion selectivity because of large pore sizes. The latter experiments

yielded  $t_H = 0.81 \pm 0.04$  (Supplementary Fig. 6), in agreement with the transport numbers known for bulk hydrochloric acid ( $t_H \approx 0.83$ ,  $t_{Cl} \approx 0.17$ )<sup>20</sup>.

## Discussion

Finally, it is instructive to compare our results with those obtained previously in conceptually similar experiments but using CVD graphene<sup>11</sup>. The latter was reported to have  $\sigma \approx 4 \text{ S cm}^{-2}$  at 1 M HCl, in clear disagreement with our experiments for mechanically exfoliated graphene, where  $\sigma$  was nearly three orders of magnitude smaller. Furthermore, no current could be detected for 1 mM HCl concentration in our experiments; however, large current densities of  $\sim 10 \text{ mA cm}^{-2}$  were reported in ref. <sup>11</sup> for CVD graphene membranes of the same area. The membrane potential reported for CVD graphene was also different, reaching only  $\sim 8 \text{ mV}$  for  $\Delta C = 10$ , or  $\sim 7$  times smaller than what we found for our devices. All this shows that the ion transport properties of exfoliated 2D crystals are radically different from those of CVD films where atomic-scale defects and, possibly, even macroscopic ones<sup>11</sup> dominate ion transport. This conclusion is consistent with all the other evidence for intrinsic proton transport through 2D crystals, which was reported previously<sup>1,2</sup>.

In conclusion, our experiments clearly demonstrate that mechanically exfoliated, defect-free 2D crystals allow only proton transport and block even small ions such as chlorine that has one of the smallest hydrated diameters<sup>19</sup>. This provides further support to the view that the activation barriers found for proton transport through high-quality graphene and hBN do not involve vacancies and other atomic-scale defects<sup>1</sup>, a conclusion important for further theory developments (e.g., for the hydrogenation model proposed in refs. <sup>8,9</sup>). Our results also have implications for the widely discussed use of atomically thin crystals as a novel platform for various separation technologies. In such technologies, selectivity is typically achieved by either perforating nanopores<sup>22–25</sup> or exploiting those naturally occurring in CVD films<sup>26,27</sup>. The fast permeation of  $\text{H}^+$  through the 2D bulk is usually ignored but can be important for designing and optimizing the membranes' properties.

## Methods

**Fabrication of 2D membranes.** Device fabrication started by isolating atomically thin layers of graphene and hBN from bulk crystals. We used hBN crystals commercially supplied by HQ Graphene. The flake was first identified optically and then characterized using atomic force microscopy and Raman spectroscopy. Supplementary Fig. 1 shows typical characterization data for one of the used hBN crystals. Similar characterization procedures were performed for graphene.

Supplementary Fig. 2 illustrates the device fabrication process. Several lithography, reactive ion etching, and wet-etching steps were performed to obtain a fully suspended SiN membrane with a  $2 \mu\text{m}$ -diameter aperture in the center. The exfoliated 2D crystals were then suspended over the apertures. The crystals were also clamped down to the SiN substrate with a polymer washer. To this end, an SU-8 photo-curable epoxy washer was prefabricated with a  $10 \mu\text{m}$ -diameter hole in the middle and transferred over the devices with the hole and aperture aligned (Supplementary Fig. 2). After the transfer, the seal was hard baked at  $150 \text{ }^\circ\text{C}$  to ensure good adhesion to the SiN substrate.

**Electrical measurements.** Devices were clamped with O-rings to separate two reservoirs filled with HCl solutions and Ag/AgCl electrodes were placed inside each reservoir. The  $I$ - $V$  characteristics were measured, applying voltages between typically  $\pm 200 \text{ mV}$  at sweep rates  $< 0.1 \text{ V min}^{-1}$ .

## Data availability

The data that support the findings of this study are available from the corresponding author upon request.

Received: 8 May 2019 Accepted: 23 August 2019

Published online: 18 September 2019

## References

- Hu, S. et al. Proton transport through one-atom-thick crystals. *Nature* **516**, 227–230 (2014).
- Lozada-Hidalgo, M. et al. Sieving hydrogen isotopes through two-dimensional crystals. *Science* **351**, 68–70 (2016).
- Miao, M., Nardelli, M. B., Wang, Q. & Liu, Y. First principles study of the permeability of graphene to hydrogen atoms. *Phys. Chem. Chem. Phys.* **15**, 16132–16137 (2013).
- Wang, W. L. & Kaxiras, E. Graphene hydrate: theoretical prediction of a new insulating form of graphene. *New J. Phys.* **12**, 125012 (2010).
- Poltavsky, I., Zheng, L., Mortazavi, M. & Tkatchenko, A. Quantum tunneling of thermal protons through pristine graphene. *J. Chem. Phys.* **148**, 204707 (2018).
- Zhang, Q., Ju, M., Chen, L. & Zeng, X. C. Differential permeability of proton isotopes through graphene and graphene analogue monolayer. *J. Phys. Chem. Lett.* **7**, 3395–3400 (2016).
- Kroes, J., Fasolino, A. & Katsnelson, M. Density functional based simulations of proton permeation of graphene and hexagonal boron nitride. *Phys. Chem. Chem. Phys.* **19**, 5813–5817 (2017).
- Feng, Y. et al. Hydrogenation facilitates proton transfer through two-dimensional honeycomb crystals. *J. Phys. Chem. Lett.* **8**, 6009–6014 (2017).
- Bartolomei, M., Hernández, M. I., Campos-Martínez, J. & Hernández-Lamóneda, R. Graphene multi-protonation: a cooperative mechanism for proton permeation. *Carbon* **144**, 724–730 (2019).
- Achtyl, J. L. et al. Aqueous proton transfer across single-layer graphene. *Nat. Commun.* **6**, 6539 (2015).
- Walker, M. I., Braeuninger-Weimer, P., Weatherup, R. S., Hofmann, S. & Keyser, U. F. Measuring the proton selectivity of graphene membranes. *Appl. Phys. Lett.* **107**, 213104 (2015).
- Gao, L. et al. Repeated growth and bubbling transfer of graphene with millimetre-size single-crystal grains using platinum. *Nat. Commun.* **3**, 699 (2012).
- Huang, P. Y. et al. Grains and grain boundaries in single-layer graphene atomic patchwork quilts. *Nature* **469**, 389–392 (2011).
- Lee, G. H. et al. High-strength chemical-vapor-deposited graphene and grain boundaries. *Science* **31**, 1073–1076 (2013).
- Bunch, J. S. et al. Impermeable atomic membranes from graphene sheets. *Nano Lett.* **8**, 2458–2462 (2008).
- Koenig, S. P., Wang, L., Pellegrino, J. & Bunch, J. S. Selective molecular sieving through porous graphene. *Nat. Nanotechnol.* **7**, 728–732 (2012).
- Wang, L. et al. Molecular valves for controlling gas phase transport made from discrete ångström-sized pores in graphene. *Nat. Nanotechnol.* **10**, 785–790 (2015).
- Kretinin, A. V. et al. Electronic properties of graphene encapsulated with different two-dimensional atomic crystals. *Nano Lett.* **14**, 3270–3276 (2014).
- Gopinadhan, K. et al. Complete steric exclusion of ions and proton transport through confined monolayer water. *Science* **11**, 145–148 (2019).
- Bard, A. J. & Faulkner, L. R. *Electrochemical Methods* (Wiley, 2001).
- Helferich, F. *Ion Exchange* (McGraw Hill, 1962).
- Wang, L. et al. Fundamental transport mechanisms, fabrication and potential applications of nanoporous atomically thin membranes. *Nat. Nanotechnol.* **12**, 509–522 (2017).
- Surwade, S. P. et al. Water desalination using nanoporous single-layer graphene. *Nat. Nanotechnol.* **10**, 459–464 (2015).
- Garaj, S. et al. Graphene as a subnanometre trans-electrode membrane. *Nature* **467**, 190–193 (2010).
- Feng, J. et al. Single-layer MoS<sub>2</sub> nanopores as nanopower generators. *Nature* **536**, 197–200 (2016).
- O'Hern, S. C. et al. Selective molecular transport through intrinsic defects in a single layer of CVD graphene. *ACS Nano* **6**, 10130–10138 (2012).
- Prozorovska, L. & Kidambi, P. R. State-of-the-art and future prospects for atomically thin membranes from 2D materials. *Adv. Mater.* **30**, 1801179 (2018).

## Acknowledgements

We acknowledge support from EPSRC-EP/N010345/1, the Lloyd's Register Foundation, the European Research Council and from Graphene Flagship. M.L.-H. acknowledges a Leverhulme Early Career Fellowship. G.-P.H. acknowledges a Marie Curie International Incoming Fellowship. L.M. acknowledges the EPSRC NowNANO program.

## Author contributions

M.L.-H. and A.K.G. designed and directed the project. L.M. fabricated devices, performed measurements, and carried out data analysis with help from S.Z., K.G., G.-P. H., and D.B. B.L.L. and H.M.C. helped with interpretation. L.M., A.K.G., and M.L.-H. wrote the manuscript. All authors contributed to discussions.

**Additional information**

**Supplementary Information** accompanies this paper at <https://doi.org/10.1038/s41467-019-12314-2>.

**Competing interests:** The authors declare no competing interests.

**Reprints and permission** information is available online at <http://npg.nature.com/reprintsandpermissions/>

**Peer review information** *Nature Communications* would like to thank Xinzhen Li and other, anonymous, reviewers for their contributions to the peer review of this work.

**Publisher's note** Springer Nature remains neutral with regard to jurisdictional claims in published maps and institutional affiliations.



**Open Access** This article is licensed under a Creative Commons Attribution 4.0 International License, which permits use, sharing, adaptation, distribution and reproduction in any medium or format, as long as you give appropriate credit to the original author(s) and the source, provide a link to the Creative Commons license, and indicate if changes were made. The images or other third party material in this article are included in the article's Creative Commons license, unless indicated otherwise in a credit line to the material. If material is not included in the article's Creative Commons license and your intended use is not permitted by statutory regulation or exceeds the permitted use, you will need to obtain permission directly from the copyright holder. To view a copy of this license, visit <http://creativecommons.org/licenses/by/4.0/>.

© The Author(s) 2019